




PAPER

A compact high-flux grating chip cold atom source

Hendrik Heine^{1,*} , Aidan S Arnold² , Melanie S Le Gonidec¹, Paul F Griffin² , Erling Riis² ,
Waldemar Herr³  and Ernst M Rasel^{1,4} 

¹ Institut für Quantenoptik, Leibniz Universität Hannover, Welfengarten 1, D-30167 Hannover, Germany

² SUPA and Department of Physics, University of Strathclyde, G4 0NG Glasgow, United Kingdom

³ Deutsches Zentrum für Luft- und Raumfahrt (DLR), Institut für Satellitengeodäsie und Intertialsensorik, Callinstr. 30B, 30167 Hannover, Germany

⁴ Laboratorium für Nano- und Quantenengineering (LNQE), Leibniz Universität Hannover, Schneiderberg 39, D-30167 Hannover, Germany

* Author to whom any correspondence should be addressed.

E-mail: heine@iqo.uni-hannover.de

Keywords: GMOT, atomchip, tophat beam, atom interferometry

OPEN ACCESS

RECEIVED
14 June 2024

REVISED
6 February 2025

ACCEPTED FOR PUBLICATION
3 March 2025

PUBLISHED
14 March 2025

Original Content from
this work may be used
under the terms of the
[Creative Commons
Attribution 4.0 licence](https://creativecommons.org/licenses/by/4.0/).

Any further distribution
of this work must
maintain attribution to
the author(s) and the title
of the work, journal
citation and DOI.



Abstract

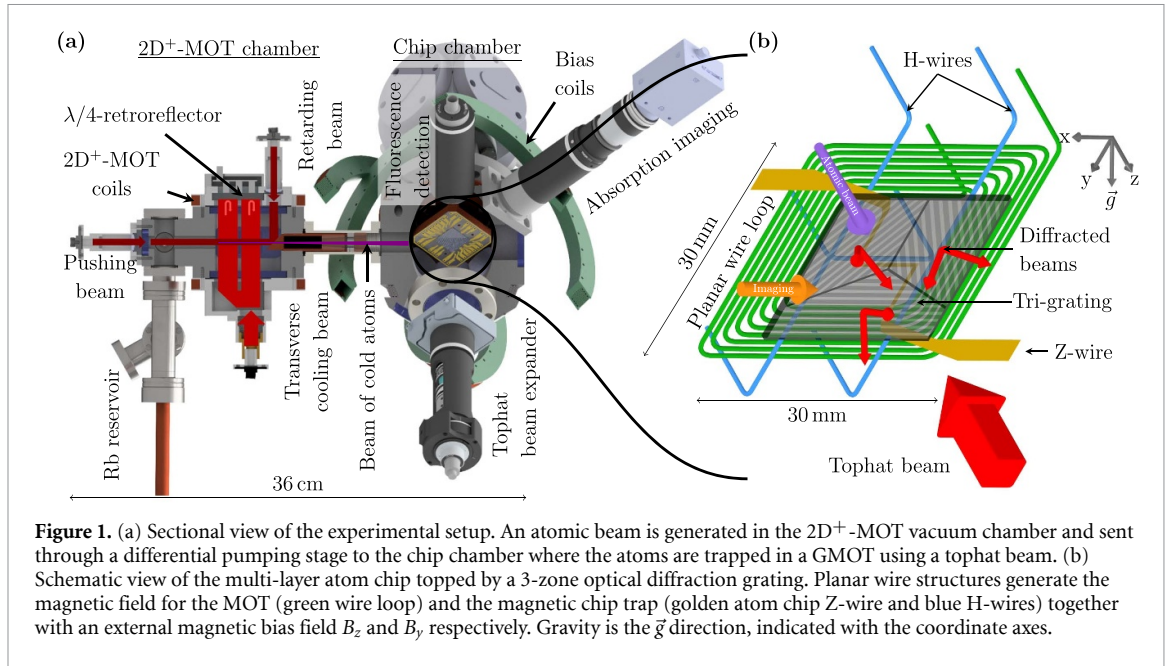
Diffraction gratings have simplified the optical implementation of magneto-optical traps (MOTs) to require only a single input beam, however reaching high atom number and fast loading has proven to be a challenge. We equipped an atom chip with a grating surface and paired it with a velocity-tunable $2D^+$ -MOT as an atomic source to facilitate efficient loading together with magnetic trapping. Using uniform grating illumination, we magneto-optically trap $1.0(1) \times 10^9$ atoms within one second, cool them to $14.1(3) \mu\text{K}$, and transfer a quarter of them into the magnetic chip trap. This is a key step towards simple portable quantum sensors employing (ultra-)cold atoms.

1. Introduction

Matter wave interferometry using (ultra-)cold atoms is useful for a wide range of applications ranging from tests of fundamental physics [1–5] to atomtronics [6, 7], searches for dark matter [8–12], Earth observation [13–19] and navigation [19–21]. Measurements employ atom-light interactions to precisely measure time and inertial forces such as acceleration and rotation using both compact [22–27] and larger devices [28–36]. Unlike their classical counterparts, quantum sensors link their measurement outcome to atomic properties and thus promise to provide an intrinsic comparability between different devices as well as long-term stability. This led to the development of mobile quantum gravimeters [15, 32, 33, 36–40] that can be operated at remote measurement sites [15, 41] where deployment complexity plays an increased role.

However, systematic effects will always affect the measurement and the ultimate accuracy is typically limited by the knowledge of conditions such as the initial kinematics of the atomic cloud, its expansion behavior and external influences [5, 33]. Achieving low temperatures and stable starting conditions of the atomic cloud is therefore a high priority in these precision measurements.

Cold atomic clouds are commonly prepared from a background gas using magneto-optical traps (MOTs [42]) and various methods of laser cooling. Ideally, the spatial and velocity distributions of the atoms in the cloud are narrow and reproducible upon release. Using Bose–Einstein condensates (BECs) as atomic sources is thus at the heart of many proposed atom interferometry missions using long evolution times [19, 43]. An important step towards simplified and robust cooling to quantum degeneracy was the invention of atom chips and magnetic micro traps [44]. Once the atoms are captured in a MOT, atom chips allow one to magnetically trap them with low electrical power and transfer them into a high-frequency trap where swift evaporative cooling to the phase transition is performed. The transfer is typically applied via an intermediate large-volume magnetic trap to capture more atoms. Overall, these methods have demonstrated a mobile high-flux BEC source [45] but still require a fairly complex optical setup which can hamper transportable deployment of the quantum sensors in-field.



In recent years, pyramidal MOTs (both regular [46–49] and tetrahedral [50–52]) as well as grating MOTs [53–59] have simplified the optical implementation of 2D and 3D-MOTs. All light fields are derived from diffraction or reflection from a single input beam, intrinsically providing stable relative intensities with low setup complexity. While regular pyramidal MOTs require bulky in-vacuum reflectors, gratings deflect the beam from a planar surface preserving the optical access. However, these systems are known to suffer from inefficient radial damping, and thereby loading, when spatially non-uniform input beam illumination is used [60–62].

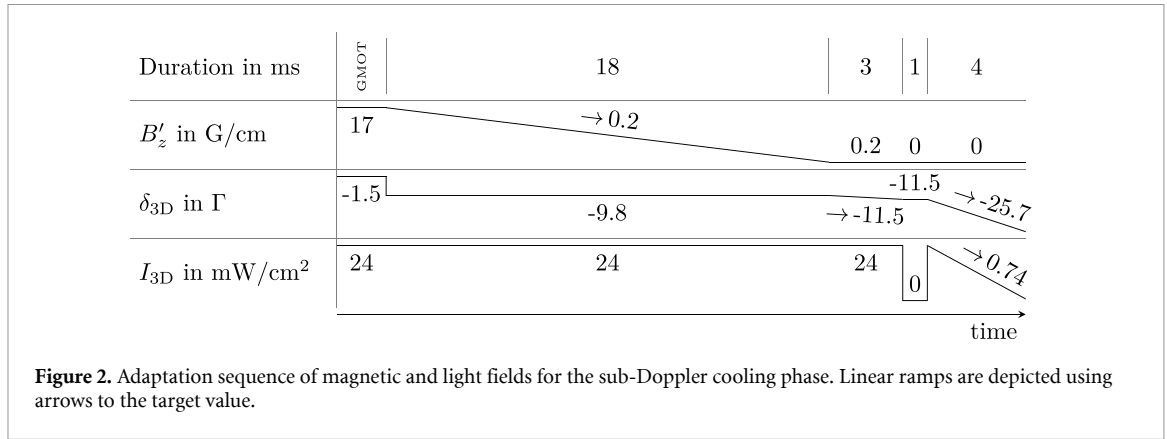
By using an atom chip with a diffraction grating surface we combine the advantages of both approaches. While the grating generates the light beams from a single input beam, the atom chip complements the assembly with fields for magnetic trapping. We use a ‘tophat’ beam with spatially uniform intensity for grating illumination and load from a differentially-pumped separate $2D^+$ -MOT [63, 64], rather than from background pressure in a single chamber [55]. With this novel combination, we set a new state-of-the-art atom number of $1.0(1) \times 10^9$ atoms in 1 s (initial MOT filling of 1.8×10^9 atoms s^{-1}) for grating MOTs and transfer $2.4(1) \times 10^8$ atoms into a large-volume magnetic trap on the chip.

2. Experimental setup

We now describe our experimental setup as depicted in figure 1. Our general-purpose atom chip testing setup comprises a double-MOT system [40, 45, 62] with a $2D^+$ -MOT [63, 64] separating the source- and atom chip chamber at different pressures. The atomic source delivers a cold atomic beam of ^{87}Rb with a tunable mean forward velocity v_1 which depends on the light detuning as well as the power and power ratio of the pushing and retarding beams. Here, the total outgoing flux is 5×10^9 atoms s^{-1} over all velocity classes with $v_1 = 20$ ms^{-1} and a FWHM velocity spread of $\Delta v_1 = 12$ ms^{-1} . The atomic beam is guided through the 1.5 mm diameter aperture of a differential pumping stage to reach the main chamber at an average height 2.7 mm above the grating surface where it is captured in a grating MOT (GMOT).

The grating atom chip assembly (figure 1(b)) is an adaption of our previous chip assemblies [40, 65] where the mirror-coated chip layer generating the high-frequency magnetic traps was replaced by a simple nano-structured chip without electrical wires. This allows us to study the most critical part of the process, which is the transfer from the GMOT into the large-volume magnetic chip trap, but sacrifices the ability to generate high-frequency magnetic traps required for efficient evaporative cooling. It consists of four main layers: The 550 μm thick top layer carries a nanostructured surface that creates all required light beams from the single incoming beam. It is followed by a 10 μm high and 500 μm wide Z-wire on the atom chip, H-wires which assist in magnetic trapping, and a planar wire loop to generate the magnetic quadrupole field for the MOT.

The nanostructure is a set of three binary diffraction gratings arranged in an equilateral triangle, detailed in [55, 66–68]. It is manufactured on a single Silicon wafer with a total grating area of 20 mm \times 20 mm and is glued with an electrically isolating epoxy (Epotek H77) on top of the Z-wire layer of the atom chip. The



binary gratings are made with a period of $d = 1080$ nm in order to diffract light with $\lambda = 780$ nm at an angle of 46° with respect to the surface normal, and an etch depth of $\lambda/4 = 195$ nm to suppress back reflection. The wafer is coated with a 100 nm thick layer of aluminum for an ideal effective power reflectivity of 33% in the first diffraction order [53]. The measured 0th order power reflectivity is 2%.

Each grating section diffracts light equally into its respective ± 1 st orders resulting in a total of 6 diffracted beams (figure 1(b)). While only the three inside diffraction orders are used for MOT with the incoming light beam, one of the outside diffracted beams partly counterpropagates with the atomic beam before it enters the central trapping area where the light forces are balanced. Crucially, this modifies the capture behavior as the atomic beam is further slowed before it is captured in the GMOT [62].

Instead of the typical Gaussian-shaped intensity profile, we use a ‘tophat’ intensity profile to evenly illuminate the nanostructure. Our custom-built beam shaper [62] utilizes two perpendicular Powell lenses to successively turn a circularly-polarized and collimated Gaussian beam into a ‘tophat’ beam featuring a $25 \text{ mm} \times 20 \text{ mm}$ rectangular area. The central plateau of $20 \text{ mm} \times 20 \text{ mm}$ fully illuminates the grating area and contains about 77% of the optical power with an average intensity fluctuation of 25% [62]. With this homogeneous illumination we estimate the volume of balanced laser cooling at 0.35 cm^3 .

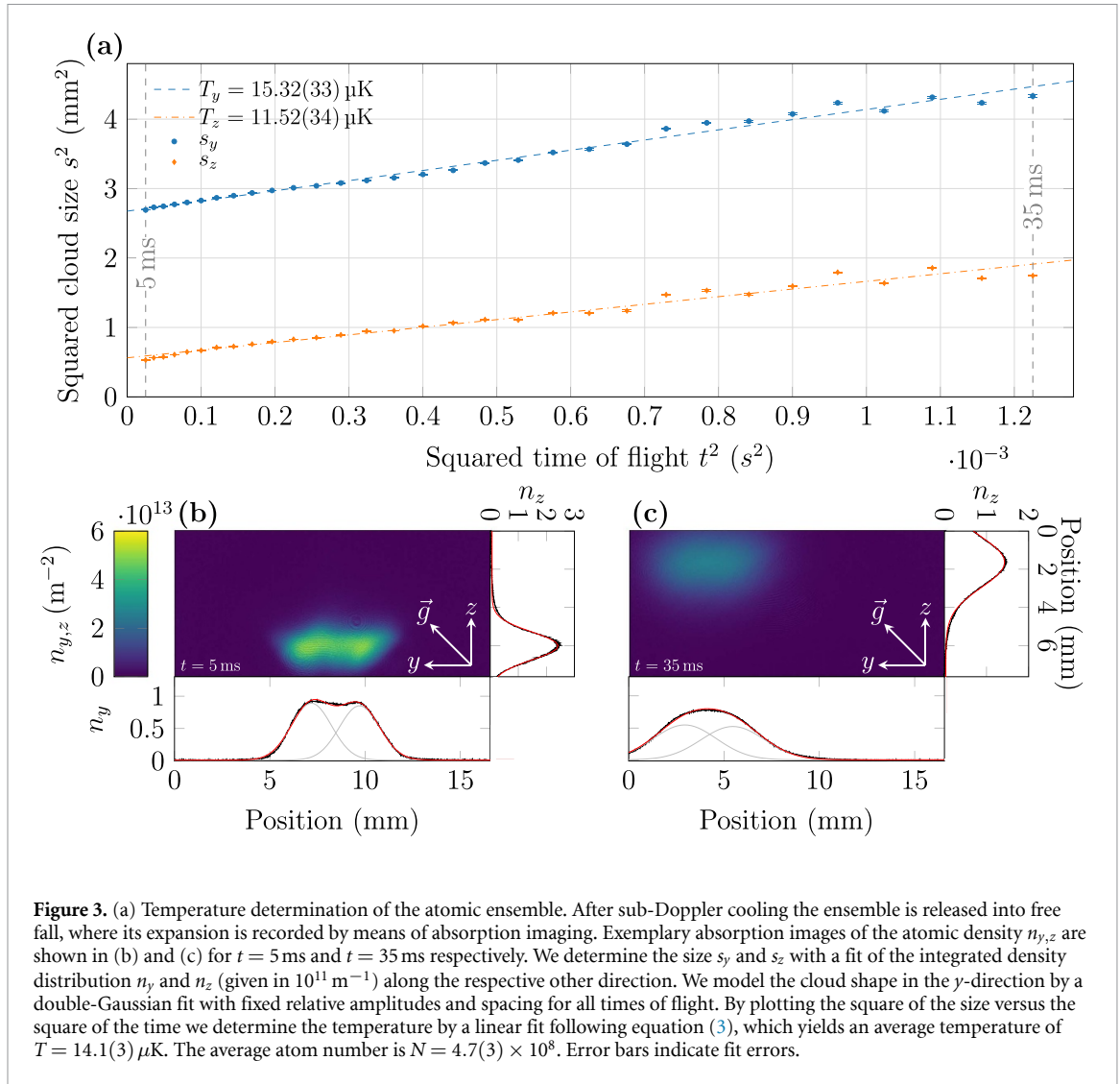
The magnetic quadrupole field of the chip MOT is generated by the planar wire loop beneath the grating (figure 1(b)) in combination with an external homogeneous bias field B_z . With this method we can generate the GMOT 5 mm above the grating surface featuring axial gradients of $B'_z = 30 \text{ G cm}^{-1}$ (300 mT m^{-1}) using only moderate currents $I_0 \leq 9.5 \text{ A}$ in the wire loop. Finally, magnetic trapping is realized with the Z-shaped atom chip structure and wires in H-configuration together with a magnetic bias field B_y to form a Ioffe–Pritchard-type magnetic chip trap [44].

3. Methods and experimental results

The following section describes the experimental parameters, methods and results. We use three offset-locked and amplified external cavity diode lasers (ECDLs) stabilized to the $5^2S_{1/2} \rightarrow 5^2P_{3/2}$ D2 line in ^{87}Rb to drive cooling ($|F = 2\rangle \rightarrow |F' = 3\rangle$) and repumping ($|F = 1\rangle \rightarrow |F' = 2\rangle$) transitions. Cooling laser powers of 450 mW (120 mW) and red-detunings of $\delta_{2D} = 24 \text{ MHz} \approx 4\Gamma$ ($\delta_{3D} = 14 \text{ MHz} \approx 2.3\Gamma$) are used for the $2D^+ - \text{MOT}$ (GMOT), where $\Gamma \approx 6 \text{ MHz}$ is the natural linewidth of the transition. Acousto-optical modulators are used for dynamic attenuation and fast switching of the light.

Loading from the well-tailored atomic source, we regularly gather $1.0(1) \times 10^9$ atoms within 1 s, using a magnetic gradient $B'_z = 26.8 \text{ G cm}^{-1}$. The magnetic field is generated by a current in the planar wire loop of $I_0 = 8 \text{ A}$ in conjunction with an external perpendicular magnetic bias field of 25.5 G. The GMOT atom number typically fluctuates within $\pm 1\%$ between experimental cycles but may drift by $\pm 10\%$ over 24 h of continuous operation (about 21 500 repetitions).

The temperature of the atomic cloud in the GMOT is about $T = 1 \text{ mK}$. Subsequent sub-Doppler cooling requires precise zeroing of the magnetic field [56, 69]. However, abruptly switching off the magnetic field of the wire loop induces eddy currents in the copper mount of the chip. Hence, we adopted a sequence (figure 2) where we operate the MOT at a lower magnetic field gradient of $B'_z = 17 \text{ G cm}^{-1}$ and a detuning of $\delta_{3D} = -1.5\Gamma$ gathering 6.0×10^8 atoms. We then ramp down the magnetic field gradient while increasing the light detuning before switching off the chip current completely. During the subsequent sub-Doppler cooling phase we null the total magnetic field and increase the light detuning linearly while decreasing the intensity over a duration of 4 ms.



We analyze the resulting velocity spread of the atomic ensemble through time-of-flight measurements using absorption imaging (see figure 3). It is evident that the initial spatial distribution of the cloud is not Gaussian along the y direction parallel to the grating surface but spatially extended (figure 3 (b)). Atomic clouds with significantly less atoms ($N \ll 1 \times 10^8$) appear Gaussian. We attribute this behavior to the densely filled MOT volume in the presence of reradiation pressure which spatially redistributes the atoms towards constant density due to inhomogeneous light forces [60, 70]. Fitting a single Gaussian to the shape of the cloud would greatly overestimate the initial size and thus underestimate the temperature. We therefore model the density distribution of the cloud with two overlaid Gaussians

$$f(x) = \frac{a}{\sqrt{2\pi}\sigma} \left(\exp \left[-\frac{(x - x_0 - \Delta x/2)^2}{2\sigma^2} \right] + \eta \exp \left[-\frac{(x - x_0 + \Delta x/2)^2}{2\sigma^2} \right] \right) \quad (1)$$

with identical standard deviation σ , where x_0 is the center of the cloud, Δx is the (fixed) separation between the Gaussians, and η is the (fixed) amplitude ratio. The generalized variance of the cloud is then calculated as

$$s^2 = \frac{\langle x^2 \rangle}{\langle x^0 \rangle} - \left(\frac{\langle x^1 \rangle}{\langle x^0 \rangle} \right)^2 = \frac{\Delta x^2 \eta}{(1 + \eta)^2} + \sigma^2 \quad (2)$$

where $\langle x^n \rangle \equiv \int x^n f(x) dx$ is the n th moment of $f(x)$. For all times of flight η and Δx are fixed based on the values from the first fit. This approach resembles the overall cloud shape very well and allows a meaningful determination of the variation of the cloud's spatial standard deviation (size s) with time. We verified this method by analyzing the second moment of the spatial distributions from the row/column-integrated densities n_y and n_z of the image but found that first fitting the distribution is more reliable as parts of the

Table 1. Comparison of dual-chamber cold atom sources from the literature where the second chamber features a grating MOT in contrast to a mobile high-flux BEC source [45] for reference. The MOT atom number is $N_{\text{MOT}} (\times 10^8 \text{ atoms})$, the MOT initial loading rate is $\phi_{\text{MOT}} (\times 10^8 \text{ atoms s}^{-1})$, the molasses temperature is $T_{\text{mol}} (\mu\text{K})$, magnetic trap loading efficiency from the MOT is η_{mag} and the flux of Bose-condensed atoms is $\phi_{\text{BEC}} (\times 10^3 \text{ atoms s}^{-1})$ with an extrapolated future performance (\dagger) based on [45] using the methods of this work. A wider source overview can be found in [49].

Source type	3D-MOT	Year	Species	N_{MOT}	ϕ_{MOT}	T_{mol}	η_{mag}	ϕ_{BEC}	References
2D ⁺ -GMOT	GMOT	2017	⁸⁷ Rb	2.5	0.8	—	—	—	[57]
Zeeman Slower	GMOT	2019	⁷ Li	0.01	0.02	—	—	—	[75]
2D-MOT	GMOT	2024	⁸⁷ Rb	2	0.7	35	>10%	5	[76]
2D ⁺ -MOT	GMOT	2024	⁸⁷ Rb	10	18	14	24%	50–100 [†]	This work
Reference performance:									
2D ⁺ -MOT	Mirror	2015	⁸⁷ Rb	10	20	20	20%	100	[45]

cloud may get cut from the field of view for longer times of flight. The fits in the perpendicular direction use a single Gaussian, as there is negligible change if the double-Gaussian method is used.

The size evolution of the cloud follows the usual ballistic expansion curve

$$s^2(t) = s_0^2 + s_v^2 t^2 \quad (3)$$

where s_0 is the initial size, t is the time of flight and $s_v^2 = \frac{k_B T}{m}$ contains the temperature T of the atomic ensemble with mass m and Boltzmann constant k_B . We find slightly different cloud expansion rates of $s_{v,y} = 38.3 \text{ mm s}^{-1}$ and $s_{v,z} = 33.2 \text{ mm s}^{-1}$ that correspond to an average temperature of $T = \frac{2}{3} T_y + \frac{1}{3} T_z = 14.1(3) \mu\text{K}$ [60] with a mean atom number $N = 4.7(3) \times 10^8$. This corresponds to a phase space density $\text{PSD} \equiv n_0 \Lambda^3 = 1.9(1) \times 10^{-6}$ where $n_0 \equiv N / ((2\pi)^{3/2} s_{0,y}^2 s_{0,z})$ is the peak atomic density for a 3D Gaussian with radial and axial widths $s_{0,y}$ and $s_{0,z}$, and Λ is the thermal de Broglie wavelength. We note that the cooling performance is limited by atom number as significantly less atoms $N \approx 1 \times 10^7$ yield lower temperatures around $T \approx 5 \mu\text{K}$, which closely follows the expected $T \propto N^{1/3}$ scaling of sub-Doppler temperature with atom number [71–74].

After sub-Doppler cooling we prepare the internal atomic state by applying optical pumping on the $|F=2\rangle \rightarrow |F'=2\rangle$ transition. Using circularly polarized light and driving σ^+ transitions, atoms accumulate into the magnetically trappable $|F=2, m_F=2\rangle$ state. Afterwards, we form a Ioffe–Pritchard type magnetic trap on the chip operating with $I_H = 10 \text{ A}$ in the H-wires and $I_Z = 5 \text{ A}$ in the atom chip Z-wire in combination with external fields B_y and B_x . Depending on the applied field, we can modify the position and properties of the trap in terms of trap depth, trap frequency and trap bottom field.

Optimizing the field for maximum atom number, we transfer up to $N_M = 2.4(1) \times 10^8$ atoms at $T = 111.1(6) \mu\text{K}$ and a PSD of $1.1(1) \times 10^{-7}$ into a trap with calculated frequencies $(\nu_{x'}, \nu_{y'}, \nu_{z'}) = (10.6, 103.4, 105.6) \text{ Hz}$. Compared to the molasses-cooled ensemble, the PSD is diminished due to the mode mismatch between the size of the cloud and the magnetic trap [45]. In contrast, optimizing for PSD, we reach $2.1(1) \times 10^{-6}$ at $N_M = 4.2(2) \times 10^7$ and $T = 18.8(2) \mu\text{K}$ for a shallower trap with calculated frequencies $(\nu_{x'}, \nu_{y'}, \nu_{z'}) = (9.3, 18.7, 27.5) \text{ Hz}$, because this trap has better mode-matching to the width of the cloud.

Efficient evaporative cooling was not possible in this setup as the device did not feature sufficient trap frequencies in comparison to the trap lifetime of $\tau = 1 \text{ s}$ to 4.4 s , depending on the specific trap. These were limited by background gas collisions which is typical for atom chip systems due to the increased local outgassing of the wire-heated surface. The achievable trap frequencies were constrained by the distance of the atoms to the wire which was obstructed by the $550 \mu\text{m}$ thick grating chip layer with the additional requirement of maintaining a non-zero trap bottom field. This is due to the fact that, compared to similar setups [40, 45, 65], the layer which generates the high-frequency magnetic traps was replaced by a plain tri-grating without wires in order to prove the basic concept. Indeed, until the final magnetic trap compression and evaporation, the performance of our grating-based cold atom source is remarkably similar to [45], and compares very favorably to other grating-based sources as seen in table 1.

4. Conclusion and discussion

In conclusion, we combined a grating MOT with an atom chip loaded from a 2D⁺-MOT, achieving a high flux of cold atoms—trapping $1.0(1) \times 10^9$ atoms in 1 s. To the best of our knowledge, this is the highest atom number and flux reported in a grating MOT so far (cf table 1), aided by balanced ‘tophat’ grating illumination which was also instrumental in efficient sub-Doppler cooling of $4.7(3) \times 10^8$ atoms to

14.1(3) μK . Transferral of $2.4(1) \times 10^8$ atoms into a large-volume magnetic chip trap was possible, however efficient evaporative cooling requires larger trap frequencies necessitating additional wires of smaller cross sections in close vicinity to the atoms.

As a next step, we will therefore replace the atom chip with an advanced version where evaporative cooling to the BEC can be applied. This can be achieved by either implementing the wires directly from the top with negligible wire width or by thinning out the thickness of the grating substrate sufficiently [76]. Indeed, in a related grating-based setup quantum degeneracy was recently reached with 5 times less MOT atoms loaded in triple the time [76]. This proves the general concept and projects a simplified transportable single-beam high-flux BEC source. With additional eddy current mitigation strategies, such as a ceramic chip holder or more sophisticated slit placement, we estimate a BEC performance similar to the current state of the art while keeping the system less complex using our methods.

These developments will be instrumental for the realization of miniaturized transportable BEC-based quantum sensors such as gyroscopes, tilt meters or gravimeters. With dedicated setups tailored to the requirements of the GMOT, the volume of the apparatus would drastically shrink. Furthermore, gratings and atom chips are both made using lithographic manufacturing techniques, making their combination into a single-substrate multi-layer chip feasible. Additional integration of photonic integrated circuits [77] and control electronics would then allow all required components for quantum sensing to be assembled into a single device with scalable manufacturing. These could be used to span networks of quantum sensors and enable future missions on ground and in space [78–80].

Data availability statement

The data that support the findings of this study are openly available at the following URL/DOI: [10.25835/C9XRYJHW](https://doi.org/10.25835/C9XRYJHW) [81].

Acknowledgments

We acknowledge support by the German Space Agency (DLR) with funds provided by the Federal Ministry of Economic Affairs and Climate Action (BMWK) due to an enactment of the German Bundestag under Grant Nos. DLR 50WM1650 (KACTUS), 50WM1947 (KACTUS II) and 50RK1976 (QCHIP). We have been funded by the Deutsche Forschungsgemeinschaft (DFG, German Research Foundation) under Germany's Excellence Strategy—EXC-2123 QuantumFrontiers - 390837967 and Project-ID 434617780 - SFB 1464 TerraQ. We acknowledge financial support from 'Niedersächsisches Vorab' through 'Förderung von Wissenschaft und Technik in Forschung und Lehre' for the initial funding of research in the new DLR-SI Institute and through the 'Quantum- and Nano-Metrology (QUANOMET)' initiative within the Project QT3. We acknowledge financial support from 'QVLS-Q1' through the VW foundation and the ministry for science and culture of Lower Saxony. Funding is appreciated from the European Space Agency (ESA) under the TRP programme, Contract No. 4000126331. We thank Maral Siercke, Amado Bautista and the group of Christian Ospelkaus for the production of parts of the atom chip assembly. ASA, PFG, and ER acknowledge support through the UK EPSRC Grant [EP/T001046/1](https://doi.org/10.13039/501100011033/EP/T001046/1), and Kelvin Nanotechnology for valuable conversations regarding integrated chip design.

ORCID iDs

Hendrik Heine  <https://orcid.org/0000-0002-3422-9001>

Aidan S Arnold  <https://orcid.org/0000-0001-7084-6958>

Paul F Griffin  <https://orcid.org/0000-0002-0134-7554>

Erling Riis  <https://orcid.org/0000-0002-3225-5302>

Waldemar Herr  <https://orcid.org/0000-0002-3685-2729>

Ernst M Rasel  <https://orcid.org/0000-0001-7861-8829>

References

- [1] Dimopoulos S, Graham P W, Hogan J M and Kasevich M A 2007 *Phys. Rev. Lett.* **98** 111102
- [2] Di Pumpo F, Ufrecht C, Friedrich A, Giese E, Schleich W P and Unruh W G 2021 *PRX Quantum* **2** 040333
- [3] Canuel B *et al* 2020 *Class. Quantum Grav.* **37** 225017
- [4] Aguilera D N *et al* 2014 *Class. Quantum Grav.* **31** 115010
- [5] Asenbaum P, Overstreet C, Kim M, Curti J and Kasevich M A 2020 *Phys. Rev. Lett.* **125** 191101
- [6] Amico L *et al* 2021 *AVS Quantum Sci.* **3** 039201
- [7] Amico L, Anderson D, Boshier M, Brantut J P, Kwek L C, Minguzzi A and von Klitzing W 2022 *Rev. Mod. Phys.* **94** 041001
- [8] Horowitz C J and Widmer-Schmid R 2020 *Phys. Rev. Lett.* **124** 051102

- [9] Derr D and Giese E 2023 *AVS Quantum Sci.* **5** 044404
- [10] Geraci A A and Derevianko A 2016 *Phys. Rev. Lett.* **117** 261301
- [11] Du Y, Murgui C, Pardo K, Wang Y and Zurek K M 2022 *Phys. Rev. D* **106** 095041
- [12] Chou A et al 2023 Quantum sensors for high energy physics (arXiv:2311.01930)
- [13] Beauflis Q et al 2023 *npj Microgravity* **9** 53
- [14] Lévêque T et al 2023 Carioqa: definition of a quantum pathfinder mission *Int. Conf. on Space Optics-ICSO 2022 (vol 12777)* (SPIE) pp 1536–45
- [15] Bidet Y, Zahzam N, Blanchard C, Bonnin A, Cadoret M, Bresson A, Rouxel D and Lequentrec-Lalancette M 2018 *Nat. Commun.* **9** 627
- [16] Lévêque T et al 2021 *J. Geod.* **95** 1–19
- [17] Carraz O, Siemes C, Massotti L, Haagmans R and Silvestrin P 2014 *Microgravity Sci. Technol.* **26** 139–45
- [18] Zahzam N et al 2022 *Remote Sens.* **14** 3273
- [19] Abend S et al 2023 *AVS Quantum Sci.* **5** 019201
- [20] Jekeli C 2005 *Navigation* **52** 1–14
- [21] Tennstedt B, Rajagopalan A, Weddig N B, Abend S, Schön S and Rasel E M 2023 *Navig. J. Inst. Navig.* **70** navi.604
- [22] Takamoto M, Ushijima I, Ohmae N, Yahagi T, Kokado K, Shinkai H and Katori H 2020 *Nat. Photon.* **14** 411–5
- [23] Stray B et al 2022 *Nature* **602** 590–4
- [24] Martinez G D, Li C, Staron A, Kitching J, Raman C and McGehee W R 2023 *Nat. Commun.* **14** 3501
- [25] Szmuk R, Dugrain V, Maineult W, Reichel J and Rosenbusch P 2015 *Phys. Rev. A* **92** 012106
- [26] Liu L et al 2018 *Nat. Commun.* **9** 2760
- [27] Roslund J D et al 2024 *Nature* **628** 736–40
- [28] Somaschi N et al 2016 *Nat. Photon.* **10** 340–5
- [29] Dutta I, Savoie D, Fang B, Venon B, Garrido Alzar C L, Geiger R and Landragin A 2016 *Phys. Rev. Lett.* **116** 183003
- [30] Morel L, Yao Z, Cladé P and Guellati-Khélifa S 2020 *Nature* **588** 61–65
- [31] Bothwell T, Kennedy C J, Aeppli A, Kedar D, Robinson J M, Oelker E, Staron A and Ye J 2022 *Nature* **602** 420–4
- [32] Bidet Y, Carraz O, Charrière R, Cadoret M, Zahzam N and Bresson A 2013 *Appl. Phys. Lett.* **102** 144107
- [33] Freier C, Hauth M, Schkolnik V, Leykauf B, Schilling M, Wziontek H, Scherneck H G, Müller J and Peters A 2016 Mobile quantum gravity sensor with unprecedented stability *J. Phys.: Conf. Ser.* **723** 012050
- [34] Fang B, Dutta I, Savoie D, Venon B, Alzar C G, Geiger R and Landragin A 2016 Cold-atom inertial sensor without deadtime 2016 *European Frequency and Time Forum (EFTF)* (IEEE) pp 1–4
- [35] Tackmann G, Berg P, Abend S, Schubert C, Ertmer W and Rasel E M 2014 *C. R. Phys.* **15** 884–97
- [36] Ménoret V, Vermeulen P, Le Moigne N, Bonvalot S, Bouyer P, Landragin A and Desruelle B 2018 *Sci. Rep.* **8** 12300
- [37] Bodart Q, Merlet S, Malossi N, Dos Santos F P, Bouyer P and Landragin A 2010 *Appl. Phys. Lett.* **96** 134101
- [38] Geiger R et al 2011 *Nat. Commun.* **2** 474
- [39] Wu B, Wang Z, Cheng B, Wang Q, Xu A and Lin Q 2014 *Metrologia* **51** 452
- [40] Heine N, Matthias J, Sahelgozin M, Herr W, Abend S, Timmen L, Müller J and Rasel E M 2020 *Eur. Phys. J. D* **74** 174
- [41] Antoni-Micollier L, Carbone D, Ménoret V, Lautier-Gaud J, King T, Greco F, Messina A, Contrafatto D and Desruelle B 2022 *Geophys. Res. Lett.* **49** e2022GL097814
- [42] Raab E L, Prentiss M, Cable A, Chu S and Pritchard D E 1987 *Phys. Rev. Lett.* **59** 2631–4
- [43] Abend S et al 2024 *AVS Quantum Sci.* **6** 024701
- [44] Reichel J, Hänsel W and Hänsch T W 1999 *Phys. Rev. Lett.* **83** 3398–401
- [45] Rudolph J et al 2015 *New J. Phys.* **17** 065001
- [46] Lee K I, Kim J A, Noh H R and Jhe W 1996 *Opt. Lett.* **21** 1177
- [47] Pollock S, Cotter J P, Lalot A, Ramirez-Martinez F and Hinds E A 2011 *New J. Phys.* **13** 043029
- [48] Bowden W, Hobson R, Hill I R, Vianello A, Schioppo M, Silva A, Margolis H S, Baird P E G and Gill P 2019 *Sci. Rep.* **9** 11704
- [49] Ravenhall S, Yuen B and Foot C 2021 *Opt. Express* **29** 21143
- [50] Vangeleyn M, Griffin P F, Riis E and Arnold A S 2009 *Opt. Express* **17** 13601
- [51] Bondza S A, Leopold T, Schwarz R and Lisdat C 2024 *Rev. Sci. Instrum.* **95** 013202
- [52] Pick J, Schwarz R, Kruse J, Lisdat C and Klempt C 2024 *Rev. Sci. Instrum.* **95** 073201
- [53] Vangeleyn M, Griffin P F, Riis E and Arnold A S 2010 *Opt. Lett.* **35** 3453
- [54] Vangeleyn M 2011 Atom trapping in non-trivial geometries for micro-fabrication applications *PhD Thesis* University of Strathclyde (<https://doi.org/10.48730/h8da-p615>)
- [55] Nshii C C, Vangeleyn M, Cotter J P, Griffin P F, Hinds E A, Ironside C N, See P, Sinclair A G, Riis E and Arnold A S 2013 *Nat. Nanotechnol.* **8** 321–4
- [56] Lee J, Grover J A, Orozco L A and Rolston S L 2013 *J. Opt. Soc. Am. B* **30** 2869
- [57] Imhof E, Stuhl B K, Kasch B, Kroese B, Olson S E and Squires M B 2017 *Phys. Rev. A* **96** 033636
- [58] Barker D S, Elgee P K, Sitaram A, Norrgard E B, Klimov N N, Campbell G K and Eckel S 2023 *New J. Phys.* **25** 103046
- [59] Calviac R, Monmayrant A, Dubreuil P, Mazonq L, Charlot S, Gauguet A, Allard B and Gauthier-Lafaye O 2024 *J. Opt. Soc. Am. B* **41** 1533–40
- [60] McGilligan J P, Griffin P F, Riis E and Arnold A S 2015 *Opt. Express* **23** 8948
- [61] McGehee W R, Zhu W, Barker D S, Westly D, Yulaev A, Klimov N, Agrawal A, Eckel S, Aksyuk V and McClelland J J 2021 *New J. Phys.* **23** 013021
- [62] Heine H 2023 A high-flux cold atom source based on a nano-structured atom chip *PhD Thesis* Leibniz Universität Hannover (<https://doi.org/10.15488/15569>)
- [63] Chaudhuri S, Roy S and Unnikrishnan C S 2006 *Phys. Rev. A* **74** 023406
- [64] Dieckmann K, Spreuw R J C, Weidemüller M and Walraven J T M 1998 *Phys. Rev. A* **58** 3891–5
- [65] Becker D et al 2018 *Nature* **562** 391–5
- [66] Cotter J P, McGilligan J P, Griffin P F, Rabey I M, Docherty K, Riis E, Arnold A S and Hinds E A 2016 *Appl. Phys. B* **122** 172
- [67] McGilligan J P, Griffin P F, Riis E and Arnold A S 2016 *J. Opt. Soc. Am. B* **33** 1271
- [68] Burrow O S, Fasano R J, Brand W, Wright M W, Li W, Ludlow A D, Riis E, Griffin P F and Arnold A S 2023 *Opt. Express* **31** 40871
- [69] McGilligan J P, Griffin P F, Elvin R, Ingleby S J, Riis E and Arnold A S 2017 *Sci. Rep.* **7** 384
- [70] Petrich W, Anderson M H, Ensher J R and Cornell E A 1994 *J. Opt. Soc. Am. B* **11** 1332–5
- [71] Hillenbrand G, Foot C J and Burnett K 1994 *Phys. Rev. A* **50** 1479–89

- [72] Hillenbrand G, Burnett K and Foot C J 1995 *Phys. Rev. A* **52** 4763–86
- [73] Ellinger K and Cooper J 1997 *Phys. Rev. A* **55** 4351–76
- [74] Drewsen M, Laurent P, Nadir A, Santarelli G, Clairon A, Castin Y, Grison D and Salomon C 1994 *Appl. Phys. B* **59** 283–98
- [75] Barker D, Norrgard E, Klimov N, Fedchak J, Scherschligt J and Eckel S 2019 *Phys. Rev. Appl.* **11** 064023
- [76] Calviac R, Rouxel A, Charlot S, Bourrier D, Arnoult A, Monmayrant A, Gauthier-Lafaye O, Gauguier A and Allard B 2025 *Phys. Rev. Appl.* **23** L011001
- [77] Isichenko A, Chauhan N, Bose D, Wang J, Kunz P D and Blumenthal D J 2023 *Nat. Commun.* **14** 3080
- [78] Trimeche A *et al* 2019 *Class. Quantum Grav.* **36** 215004
- [79] Schubert C, Abend S, Gersemann M, Gebbe M, Schlippert D, Berg P and Rasel E M 2021 *Sci. Rep.* **11** 16121
- [80] Loriani S *et al* 2019 *New J. Phys.* **21** 063030
- [81] Heine H 2025 Datasets to ‘A compact high-flux grating chip cold atom source’ *LUIS* (<https://doi.org/10.25835/C9XRYJHW>)